

AD-A134 739

ASSESSMENT OF REAL GAS EFFECTS ON THE PREDICTION OF THE
AERODYNAMICS OF H. (U) THERMAL SCIENCES INC SUNNYVALE
CA* W E NICOLET ET AL. SEP 83 ARBRL-CR-00517

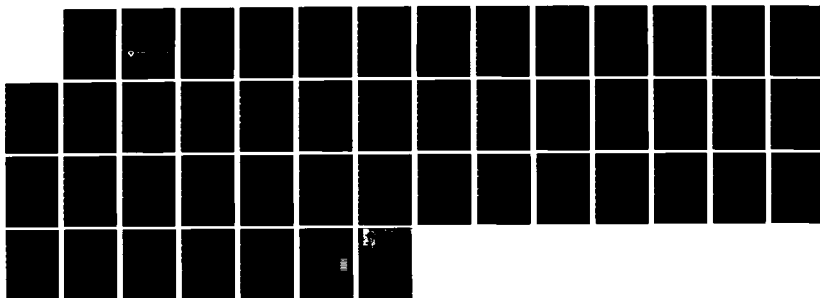
1/1

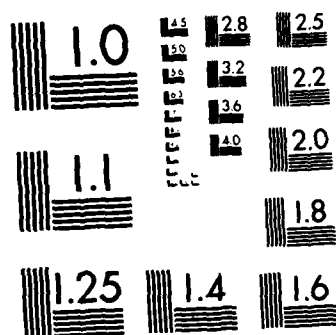
UNCLASSIFIED

DAAG29-81-D-0100

F/G 20/4

NL





MICROCOPY RESOLUTION TEST CHART
NATIONAL BUREAU OF STANDARDS-1963-A

1-2

AD-A134 739

AD


CONTRACT REPORT ARBRL-CR-00517

ASSESSMENT OF REAL GAS EFFECTS ON THE
PREDICTION OF THE AERODYNAMICS OF
HIGH VELOCITY ARMY SHELLS

Prepared by

Thermal Sciences, Inc.
292 Gibraltar Drive, Suite A-4
Sunnyvale, California 94086

September 1983



US ARMY ARMAMENT RESEARCH AND DEVELOPMENT COMMAND
BALLISTIC RESEARCH LABORATORY
ABERDEEN PROVING GROUND, MARYLAND

Approved for public release; distribution unlimited.

DTIC
ELECTRONIC
NOV 3 1983

DTIC FILE COPY

83 11 03 017

Destroy this report when it is no longer needed.
Do not return it to the originator.

Additional copies of this report may be obtained
from the National Technical Information Service,
U. S. Department of Commerce, Springfield, Virginia
22161.

The findings in this report are not to be construed as
an official Department of the Army position, unless
so designated by other authorized documents.

*The use of trade names or manufacturers' names in this report
does not constitute endorsement of any commercial product.*

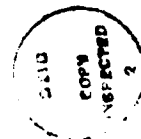
UNCLASSIFIED

SECURITY CLASSIFICATION OF THIS PAGE (When Data Entered)

REPORT DOCUMENTATION PAGE		READ INSTRUCTIONS BEFORE COMPLETING FORM
1. REPORT NUMBER CONTRACT REPORT ARBRL-CR-00517	2. GOVT ACCESSION NO. AD-A134 739	3. RECIPIENT'S CATALOG NUMBER
4. TITLE (and Subtitle) ASSESSMENT OF REAL GAS EFFECTS ON THE PREDICTION OF THE AERODYNAMICS OF HIGH VELOCITY ARMY SHELLS		5. TYPE OF REPORT & PERIOD COVERED Final
		6. PERFORMING ORG. REPORT NUMBER
7. AUTHOR(s) W. E. Nicolet and G.R. Srinivasan		8. CONTRACT OR GRANT NUMBER(s) DAAG29-81-D-0100
9. PERFORMING ORGANIZATION NAME AND ADDRESS Thermal Sciences, Inc. 292 Gibraltar Dr., Suite A-4 Sunnyvale, CA 94086		10. PROGRAM ELEMENT, PROJECT, TASK AREA & WORK UNIT NUMBERS RDT&E 1L162618AH80
11. CONTROLLING OFFICE NAME AND ADDRESS US Army Armament Research & Development Command US Army Ballistic Research Laboratory (DRDAR-BLA-S) Aberdeen Proving Ground, MD 21005		12. REPORT DATE September 1983
		13. NUMBER OF PAGES 45
14. MONITORING AGENCY NAME & ADDRESS (if different from Controlling Office)		15. SECURITY CLASS. (of this report) Unclassified
		15a. DECLASSIFICATION/DOWNGRADING SCHEDULE
16. DISTRIBUTION STATEMENT (of this Report) Approved for public release; distribution unlimited.		
17. DISTRIBUTION STATEMENT (of the abstract entered in Block 20, if different from Report)		
18. SUPPLEMENTARY NOTES This work was performed under the direction of the Aerodynamics Research Branch, Launch and Flight Division, DRDAR-BLL, Dr. Walter B. Sturek, Contracting Officer's Technical Representative.		
19. KEY WORDS (Continue on reverse side if necessary and identify by block number) Hypersonic Flow Projectile Aerodynamics Computational Aerodynamics Real Gas Effects		
20. ABSTRACT (Continue on reverse side if necessary and identify by block number) The present study assesses real gas effects in the prediction of flow- fields over Army projectiles. Solutions are obtained for a spherically tipped cone-cylinder model flying at three different flight conditions. Real gas effects may be important for the pressure and heat transfer on the spherical tip. Real gas effects are not important for the prediction of pressure and heat transfer on the region of the model aft of the spherical tip.		

TABLE OF CONTENTS

	<u>Page</u>
LIST OF ILLUSTRATIONS.....	5
I. INTRODUCTION.....	7
II. REAL GAS TERMS.....	9
1. Equation of State.....	9
2. The \hat{S} Matrix.....	11
3. Jacobian Matrices.....	16
4. Shock Fitting.....	19
5. Implementation in PNS Code.....	25
III. CALCULATIONS.....	27
1. Model Geometry.....	27
2. Flight Conditions.....	27
3. Surface Grid.....	28
4. Starting Conditions.....	28
5. Downstream Solutions.....	28
IV. CONCLUDING REMARKS.....	32
REFERENCES.....	42
DISTRIBUTION LIST.....	43



LIST OF ILLUSTRATIONS

<u>Figure</u>		<u>Page</u>
1	Shock Wave Notation.....	33
2	Pressure Distribution on 7° Sphere Cone at $\alpha = 0^\circ$ from Harris ⁷ ..	34
3	Pressure Distribution for Case 3 (M = 10) Showing Real Gas Effects for Laminar Flow.....	35
4	Pressure Distribution for Case 3 (M = 10) Showing Real Gas Effects for Turbulent Flow.....	36
5	Heat Transfer for Case 3 (M = 10) Showing Real Gas Effects for Laminar Flow.....	37
6	Heat Transfer for Case 3 (M = 10) Showing Real Gas Effects for Turbulent Flow.....	38
7	Temperature Distribution Across Shock Layer for x = 2.053 Inches at Windward Pitch Plane (Case 3).....	39
8	Real Gas Axial Pressure Distribution for Cases 1, 2 and 3.....	40
9	Real Gas Circumferential Pressure Distribution at x = 11.2 Inches for Cases 1, 2 and 3.....	41

SECTION I

INTRODUCTION

There is a continuing interest on the part of the U. S. Army in fin-stabilized vehicles designed to fly at low altitudes and hypersonic velocities. Various missiles operate in this flight regime as do the high energy, sabot-launched projectiles (KE penetrators) used to penetrate heavy armored vehicles.

The flight environments (surface shear, heat transfer and pressure) needed to support design activities traditionally have been obtained by correlating laboratory or range data and extrapolating to flight conditions. It is now recognized that finite difference methods may supplement or supplant the traditional empirical approaches and offer both a better understanding of the flowfields and a potentially significant reduction in design costs. The use of finite difference methods for this application is being assessed and explored via a number of ongoing studies at various research organizations.

Most current flowfield models consist of one of several alternative sets of flowfield equations, a perfect gas equation of state and simple correlations or tables for the properties (viscosity, specific heat and Prandtl Number). Such perfect or ideal gas formulations are valid for air flowfields provided that (1) the Mach numbers are not high enough to cause significant dissociation, (2) there are no condensibles in the flow and (3) there is no source of non-air elements within the flow. Real gas effects can be important and should be included in the formulation when any of these constraints are not satisfied.

The real gas terms associated with dissociation enter the flowfield

model via the equation of state and the thermodynamic and transport properties. These terms were formulated and included in an automated solution procedure for the parabolized Navier-Stokes equations on a previous study for AFWAL¹. This solution procedure is used in the present study to assess the significance of real gas effects on the predicted flowfields about typical fin-stabilized vehicles flying at hypersonic velocities and low altitudes.

Flowfield predictions have been obtained at (or near) standard atmospheric conditions for three Mach Numbers ($M=6, 8$ and 10). The vehicle considered consists of a spherically tipped small half angle cone joined to a cylindrical afterbody. Predictions were made both with and without real gas effects to allow a direct assessment of real gas effects on the aerodynamic and aerothermodynamic environments.

The following sections discuss (1) the real gas parabolized Navier-Stokes flowfield model, (2) the calculations performed as part of the present study and (3) the conclusions reached as a result of the present study.

SECTION II

REAL GAS TERMS

Real gas terms enter the parabolized Navier-Stokes relations² via the equation of state, the shock fitting logic, the \hat{S} matrix and the Jacobian matrices \hat{A} , \hat{B} , \hat{C} , \hat{M} , and A_u , where the terminology has been defined previously.² Perfect gas approximations are also currently employed in the calculation of the speed of sound. Modifications to the present formulation for each of these areas will be discussed in the following paragraphs.

1. Equation of State

The conservation equations are written in terms of an energy variable e_T defined as a total (internal plus kinetic) energy per unit volume.* In terms of commonly employed thermodynamic variables, e_T can be written as

$$e_T = \rho e + \rho[u^2 + v^2 + w^2]/2 \quad (1)$$

where e is the specific internal energy (energy per unit mass). For a perfect gas $\rho e = p/(\gamma-1)$, and Eq. (1) reduces to the form usually seen in the literature

$$e_T = \frac{p}{\gamma-1} + \rho[u^2 + v^2 + w^2]/2 \quad (2)$$

*Most authors designate the total internal per unit volume as e . The change to e_T here was done to avoid confusion with the specific internal energy, needed to describe real gas flows.

For a real gas having constant elemental composition,

$$e = \phi(p, \rho) \frac{p}{\rho} \quad (3)$$

where $\phi(p, \rho)$ is a function which must be determined numerically. Substituting Eq. (3) into Eq. (1) yields

$$e_T = \phi(p, \rho) p + \rho[u^2 + v^2 + w^2]/2 \quad (4)$$

which now properly includes real gas effects. Note that Eq. (4) is nonlinear in pressure in contrast to Eq. (2). Methods for obtaining pressure from Eq. (4) will be discussed subsequently.

The partial derivatives of pressure with respect to the elements (q) of the \hat{U} matrix (i.e., ρ , ρu , ρv , ρw , e_T) will be needed in forming the Jacobian matrices. It is convenient to obtain them now by taking the total derivative of Eq. (4). Thus,

$$de_T = \left(\phi + p \frac{\partial \phi}{\partial p} \right) dp - \left[u^2 + v^2 + w^2 - 2p \frac{\partial \phi}{\partial \rho} \right] \frac{d\rho}{2} + u d(\rho u) + v d(\rho v) + w d(\rho w) \quad (5)$$

The partial derivatives of pressure are easily extracted from Eq. (5) as

$$\frac{\partial p}{\partial \rho} = +0.5 \left[u^2 + v^2 + w^2 - 2p \frac{\partial \phi}{\partial \rho} \right] / \left(\phi + p \frac{\partial \phi}{\partial p} \right) \quad (6a)$$

$$\frac{\partial p}{\partial (\rho u)} = -u / \left(\phi + p \frac{\partial \phi}{\partial p} \right) \quad (6b)$$

$$\frac{\partial p}{\partial (\rho v)} = -v / \left(\phi + p \frac{\partial \phi}{\partial p} \right) \quad (6c)$$

$$\frac{\partial p}{\partial (\rho w)} = -w / \left(\phi + p \frac{\partial \phi}{\partial p} \right) \quad (6d)$$

$$\frac{\partial p}{\partial e_T} = 1/\left(\phi + p \frac{\partial \phi}{\partial p}\right) \quad (6e)$$

which completes the formulation of the new pressure partial derivatives for the Jacobian matrices.

2. The \hat{S} Matrix

The elements of the \hat{S} matrix represent the terms on the right side of the conservation equations. The perfect gas formulation is correct for the continuity and momentum equations for any thin-layer flow. However, the energy equation includes a flux divergence term on the right side which includes two key relations applicable only to perfect or ideal gases. Revision of the formulation starts with a generally valid form of the flux divergence term (FDT) which can be written as

$$FDT = - \frac{L}{\rho_r U_r^3} \left(\frac{\partial q}{\partial y} \right) \quad (7)$$

where Cartesian coordinates are employed and q is the flux, y is the coordinate in the wall normal direction and ρ_r , U_r , and L are reference values of density, velocity and length used to nondimensionalize the equation. In the perfect gas formulation, the relations

$$q = -k \frac{\partial T}{\partial y} \quad (8)$$

and

$$c_p T = \frac{a^2}{\gamma - 1} \quad (9)$$

are used to reduce Eq. (7) to the form

$$FDT = \frac{1}{Re} \frac{\partial}{\partial y} \left[\frac{\tilde{K}}{\tilde{Pr}} \frac{\partial (\tilde{a})^2}{\partial y} \right] \quad (10)$$

where nondimensional variables are used exclusively and are defined as follows:

$$\tilde{e}_T = e_T / \rho_r U_r^2$$

$$\tilde{t} = t / (L / U_r)$$

$$\tilde{K} = k / k_r$$

$$Re = \rho_r U_r L / \mu_r \text{ (Reynolds number)}$$

$$Pr = \mu_r C_{p_f} / k_r \text{ (Prandtl number)}$$

$$U_r = a_\infty$$

$$\tilde{a} = a / U_r \text{ (sound speed)}$$

where C_{p_f} is taken as the specific heat at a constant pressure for the perfect or ideal gas. This variable will be redefined subsequently for real gas as the frozen specific heat (hence the f subscript).

The real gas analog of Eq. (8) must include chemical changes in the gas and the associated effects of diffusion. The heat flux becomes

$$q = -k \frac{\partial T}{\partial y} + \sum_{\text{species}} j_i h_i \quad (11)$$

where the summation is taken over all the species present in the gas, j_i is the mass flux of the i^{th} species and h_i is the species enthalpy (energy per unit mass) and is well approximated as being a function of temperature only $h_i = h_i(T)$.

The mass flux terms appearing in Eq. (11) can be formulated by introducing Fick's law and employing the binary diffusion approximation. Thus,

$$j_i = -\rho D \frac{\partial k_i}{\partial y} \quad (12)$$

where D is the binary diffusion coefficient and k_i is the mass fraction of the i^{th} species. Substituting Eq. (12) and j_i in Eq. (11) yields the heat flux q as

$$q = -k \frac{\partial T}{\partial y} - \rho D \sum_{\text{species}} h_i \frac{\partial k_i}{\partial y} \quad (13)$$

which is further simplified to

$$q = -k \frac{\partial T}{\partial y} - \rho D \left[\frac{\partial h}{\partial y} - c_{p_f} \frac{\partial T}{\partial y} \right] \quad (14)$$

In obtaining Eq. (14) from Eq. (13), the following definitions and identities have been employed:

$$h \equiv \sum k_i h_i \quad (15)$$

$$c_{p_f} \equiv \sum k_i c_{p_i} \text{ (frozen specific heat)} \quad (16)$$

$$\sum_{\text{species}} k_i \frac{\partial h_i}{\partial y} = \frac{\partial T}{\partial y} \sum_{\text{species}} k_i c_{p_i} \quad (17)$$

$$\sum_{\text{species}} h_i \frac{\partial k_i}{\partial y} = \frac{\partial}{\partial y} \sum_{\text{species}} k_i h_i - \sum_{\text{species}} k_i \frac{\partial h_i}{\partial y} \quad (18)$$

The Schmidt number Sc defined as

$$Sc \equiv \frac{\nu}{\rho D} \quad (19)$$

is usually employed to reduce Eq. (14) to the form

$$q = -\frac{\nu}{Sc} \left[\frac{\partial h}{\partial y} + \left(\frac{Sc}{Pr} - 1 \right) c_{p_f} \frac{\partial T}{\partial y} \right] \quad (20)$$

which is in a form suitable for nondimensionalization and subsequent evaluation.

Turbulence terms can be included in the heat flux formulation by adding turbulence contributions to the thermal conductivity and diffusion coefficient. Equation (13) with turbulence becomes

$$q = -(k + \rho \epsilon_H c_{p_f}) \frac{\partial T}{\partial y} - \rho(\mathcal{D} + \epsilon_D) \left[\frac{\partial h}{\partial y} - c_{p_f} \frac{\partial T}{\partial y} \right] \quad (21)$$

where ϵ_H is the eddy conductivity, ϵ_D is the eddy diffusivity and both are related to the eddy viscosity ϵ_M via the relations

$$\epsilon_H = \frac{\epsilon_M}{Pr_t} \quad (22)$$

$$\epsilon_D = \frac{\epsilon_M}{Sc_t}$$

where Pr_t and Sc_t are the turbulent Prandtl and Schmidt numbers, respectively. The generalized form of Eq. (20) which includes turbulence effects is readily obtained as

$$q = -\frac{\mu}{Sc} \left[\frac{\partial h}{\partial y} + \left(\frac{Sc}{Pr} - 1 \right) c_{p_f} \frac{\partial T}{\partial y} \right] - \frac{\rho \epsilon_M}{Sc_t} \left[\frac{\partial h}{\partial y} + \left(\frac{Sc_t}{Pr_t} - 1 \right) c_{p_f} \frac{\partial T}{\partial y} \right] \quad (23)$$

This equation can be simplified into the commonly used effective conductivity form, i.e.

$$q = -k_{eff} \frac{\partial T}{\partial y}$$

for flows having constant elemental composition and negligible pressure gradients in the y direction. Generally, these are valid constraints in the region near a wall where heating rate is important provided there is no source of foreign elements at the wall (via blowing, transpiration, ablation, etc.). Thus, the enthalpy gradient can be written as

$$\frac{\partial h}{\partial y} = c_{p_e} \frac{\partial T}{\partial y}$$

where c_{p_e} is the equilibrium specific heat. Substituting this relation into Equation (23) yields a definition for the k_{eff} .

$$k_{eff} = \frac{\mu}{Sc} \left[c_{p_e} + \left(\frac{Sc}{Pr} - 1 \right) c_{p_f} \right] + \frac{\rho \epsilon_M}{Sc_t} \left[c_{p_e} + \left(\frac{Sc_t}{Pr_t} - 1 \right) c_{p_f} \right] \quad (24)$$

which is in its final form prior to the introduction of nondimensional variables.

The additional nondimensional variables needed are defined as

$$\tilde{c}_{p_f} \equiv c_{p_f} T_r / u_r^2$$

$$\tilde{c}_{p_e} \equiv c_{p_e} T_r / u_r^2$$

$$\tilde{T} \equiv T / T_r$$

$$\tilde{\epsilon}_M \equiv \rho_r \epsilon_M / u_r$$

$$\tilde{h} \equiv h / u_r^2$$

Substituting these relations into Eq. (24) and rearranging terms yields

$$FDT = \frac{1}{Re} \frac{\partial}{\partial y} \left\{ \left(\frac{\mu}{Sc} + \frac{\tilde{\rho} \tilde{\epsilon}_M}{Sc_t} \right) \tilde{c}_{p_e} + \left[\frac{\mu}{Sc} \left(\frac{Sc}{Pr} - 1 \right) + \frac{\tilde{\rho} \tilde{\epsilon}_M}{Sc_t} \left(\frac{Sc_t}{Pr_t} - 1 \right) \right] \tilde{c}_{p_f} \right\} \frac{\partial \tilde{T}}{\partial y} \quad (25)$$

Finally, Eq. (25) is transformed to generalized spatial coordinates to yield

$$FDT = \left[(\zeta_x^2 + \zeta_y^2 + \zeta_z^2) J^{-1} \right] \left\{ \left(\frac{\mu}{Sc} + \frac{\tilde{\rho} \tilde{\epsilon}_M}{Sc_t} \right) \tilde{c}_{p_e} + \left[\frac{\mu}{Sc} \left(\frac{Sc}{Pr} - 1 \right) + \frac{\tilde{\rho} \tilde{\epsilon}_M}{Sc_t} \left(\frac{Sc_t}{Pr_t} - 1 \right) \right] \tilde{c}_{p_f} \right\} \tilde{T}_{,\xi} \zeta \quad (26)$$

to be used in place of the existing term, i.e.,

$$FDT = \left[(\zeta_x^2 + \zeta_y^2 + \zeta_z^2) J^{-1} K Pr^{-1} (\gamma - 1)^{-1} (a^2)_{\zeta} \right]_{\zeta} \quad (27)$$

where the Reynolds number has been factored out of both Eqs. (26) and (27) and appears elsewhere in the conservation equation.

Equation (26) has two terms of the form $a_{\zeta} \phi \delta_{\zeta} \psi$, each of which is differenced as

$$\delta_{\zeta} \phi \delta_{\zeta} \psi = \frac{(\phi_{l+1} + \phi_l)(\psi_{l+1} - \psi_l) - (\phi_l + \phi_{l-1})(\psi_l - \psi_{l-1})}{2\Delta\zeta^2} \quad (28)$$

which is the same difference equation presently used to evaluate Eq. (27). The linearity of Eq. (28) is retained by lagging the property evaluation -- i.e., using properties evaluated at the previous time (or space) step. This allows the procedure developed for the perfect gas formulation to be employed here.

3. Jacobian Matrices

The first three of the Jacobian matrices to be considered are of the form

$$\hat{A} = J^{-1} [a \hat{\theta}(U, \xi) / a \hat{U}] \quad (29a)$$

$$\hat{B} = J^{-1} [a \hat{\theta}(V, \eta) / a \hat{U}] \quad (29b)$$

$$\hat{C} = J^{-1} [a \hat{\theta}(W, \xi) / a \hat{U}] \quad (29c)$$

where

$$\hat{\theta}(\alpha, \beta) = \begin{bmatrix} \rho \alpha \\ \rho u \alpha + \beta_x p \\ \rho v \alpha + \beta_y p \\ \rho w \alpha + \beta_z p \\ (e_T + p) \alpha - \beta_t p \end{bmatrix} \quad (30)$$

Real gas effects impact the partial derivative terms only via terms of the form

$$\frac{\partial \hat{\Theta}(\alpha, \beta)}{\partial p}$$

which are readily obtained from the relations presented in Eq. (6).

The \hat{M}_R matrix is the Jacobian of the real gas analog of the \hat{S} matrix (which we will relabel as \hat{S}_R). The formulation is

$$\hat{M}_R = J^{-1} [\partial \hat{S}_R / \partial \hat{U}] \quad (31)$$

where

$$\hat{S}_R = J^{-1} \begin{pmatrix} 0 \\ \tilde{u}(\zeta_x^2 + \zeta_y^2 + \zeta_z^2)\tilde{u}_\zeta + \left(\frac{\tilde{u}}{3}\right)(\zeta_x\tilde{u}_\zeta + \zeta_y\tilde{v}_\zeta + \zeta_z\tilde{w}_\zeta)\zeta_x \\ \tilde{u}(\zeta_x^2 + \zeta_y^2 + \zeta_z^2)\tilde{v}_\zeta + \left(\frac{\tilde{u}}{3}\right)(\zeta_x\tilde{u}_\zeta + \zeta_y\tilde{v}_\zeta + \zeta_z\tilde{w}_\zeta)\zeta_y \\ \tilde{u}(\zeta_x^2 + \zeta_y^2 + \zeta_z^2)\tilde{w}_\zeta + \left(\frac{\tilde{u}}{3}\right)(\zeta_x\tilde{u}_\zeta + \zeta_y\tilde{v}_\zeta + \zeta_z\tilde{w}_\zeta)\zeta_z \\ (\zeta_x^2 + \zeta_y^2 + \zeta_z^2)(0.5\tilde{u}(\tilde{u}^2 + \tilde{v}^2 + \tilde{w}^2) \\ + \left\{ \left(\frac{\tilde{u}}{Sc} + \frac{\tilde{\rho} \epsilon_M}{Sc_t}\right)\tilde{c}_{p_e} + \left[\frac{\tilde{u}}{Sc} \left(\frac{Sc}{Pr} - 1\right) + \frac{\tilde{\rho} \epsilon_M}{Sc_t} \left(\frac{Sc_t}{Pr_t} - 1\right) \right] \tilde{c}_{p_f} \right\} \tilde{T}_\zeta \\ + \left(\frac{\tilde{u}}{3}\right)(\zeta_x\tilde{u} + \zeta_y\tilde{v} + \zeta_z\tilde{w})(\zeta_x\tilde{u}_\zeta + \zeta_y\tilde{v}_\zeta + \zeta_z\tilde{w}_\zeta) \end{pmatrix} \quad (32)$$

The top four elements in \hat{S}_R [$\hat{S}_R(1)$, $\hat{S}_R(2)$, $\hat{S}_R(3)$, and $\hat{S}_R(4)$] are identical to the top four elements in \hat{S} and need not be modified. The bottom element $\hat{S}_R(5)$ contains the real gas contribution to the flux divergence and is significantly different from the corresponding element $\hat{S}(5)$.

Derivatives of the various thermodynamic and transport properties are required in order to support evaluation of the $\partial \hat{S}_R / \partial \hat{U}$ elements appearing in the \hat{M}_R matrix. The properties in question include T , h , u , Sc , C_{p_f} , and Pr . The turbulent Prandtl and Schmidt numbers will be taken to be constants ($Pr_t = 0.9$, $Sc_t = 0.9$), while the eddy viscosity is dealt with separately.

Let $\lambda(p, \rho)$ represent any one of the properties of interest (i.e., T , h , u , . . .). The chain rule is used to obtain the total derivative

$$d\lambda = \left. \frac{\partial \lambda}{\partial p} \right|_{\rho} dp + \left. \frac{\partial \lambda}{\partial \rho} \right|_{p} d\rho$$

allowing $d\rho$ to be obtained, i.e.

$$d\rho = (d\lambda - \left. \frac{\partial \lambda}{\partial p} \right|_{\rho} dp) / \left(\left. \frac{\partial \lambda}{\partial \rho} \right|_{p} \right) \quad (33)$$

and substituting this result into Eq. (5) to obtain

$$de_T = R d\lambda - \left[u^2 + v^2 + w^2 - 2p \left. \frac{\partial \phi}{\partial p} \right|_{\rho} + 2R \left. \frac{\partial \lambda}{\partial \rho} \right|_{p} \right] \frac{d\rho}{2} + u d(\rho u) + v d(\rho v) + w d(\rho w) \quad (34)$$

where

$$R \equiv \frac{\phi + \left. \frac{\partial \phi}{\partial \ln p} \right|_{\rho}}{\left. \frac{\partial \lambda}{\partial \rho} \right|_{p}} \quad (35)$$

Eq. (34) can be used to generate all of the partial derivatives for each of the properties. Thus,

$$\left. \frac{\partial \lambda}{\partial p} \right|_{\rho u, \rho v, \rho w, e_T} = \frac{1}{2R} \left[u^2 + v^2 + w^2 - 2p \left. \frac{\partial \phi}{\partial p} \right|_{\rho} + 2R \left. \frac{\partial \lambda}{\partial \rho} \right|_{p} \right] \quad (36)$$

$$\left. \frac{\partial \lambda}{\partial \rho u} \right|_{p, \rho v, \rho w, e_T} = -\frac{u}{R} \quad (37)$$

$$\left. \frac{\partial \lambda}{\partial \rho v} \right|_{\rho, \rho u, \rho w, e_T} = - \frac{v}{R} \quad (38)$$

$$\left. \frac{\partial \lambda}{\partial \rho w} \right|_{\rho, \rho u, \rho v, e_T} = - \frac{w}{R} \quad (39)$$

$$\left. \frac{\partial \lambda}{\partial e_T} \right|_{\rho, \rho u, \rho v, \rho w} = \frac{1}{R} \quad (40)$$

which completes the formulation of the property derivatives.

The partial derivatives $\partial \hat{S}_R / \partial \hat{U}$ are obtained by substituting finite difference relations for the quantities $\tilde{u}_\zeta, \tilde{v}_\zeta, \tilde{w}_\zeta, \tilde{h}_\zeta, \tilde{T}_\zeta$ then using the chain rule on the resulting expression. This is a straightforward operation yielding a lengthy result which will not be presented here.

4. Shock Fitting

Shock fitting procedures are employed in the evaluation of both unsteady and steady-state supersonic flows to determine the position of the bow shock wave and some of the flow and thermodynamic variables behind it. Initially, the pressure behind the bow shock (p_2) is obtained by explicitly integrating a combination of the equations of motion from the wall to the shock. Knowing p_2 allows the shock velocity (unsteady flows) or slope (steady-state flows) to be determined from the Rankine-Hugoniot relations. The variable (shock velocity or slope) obtained from this evaluation is then used to obtain the new shock position by propagating the shock in the ζ -direction along constant ξ and η lines. Real gas effects enter the formulations via the Rankine-Hugoniot relations. The details follow for both the unsteady and steady-state shock fitting procedures.

In the unsteady flow formulation, the shock is allowed to move outward away from the body with a velocity \overline{q}_s in the shock normal direction. The sign conventions for q_s and the other important velocity components are shown in Fig. 1. The shock velocity is given by the relation

$$\overline{q}_s = \overline{u}_{ss_1} + \tilde{u}_1 \quad (41)$$

where \tilde{u}_1 is the component of the freestream velocity vector \overline{q}_1 directed toward the shock along the shock normal, and \overline{u}_{ss_1} is the velocity vector the shock would have if \overline{q}_1 were set to zero while holding p_2/p_1 fixed. The vector $-\overline{u}_{ss_1}$ can also be viewed as the freestream velocity component in the shock normal direction required to maintain a steady-state shock wave of pressure ratio p_2/p_1 .

The unknown velocity vectors are obtained by simple manipulation of the vector relations starting with \tilde{u}_1 which is obtained by

$$\tilde{u}_1 = \overline{q}_1 \cdot \overline{n}_s \quad (42)$$

where \overline{n}_s is the unit vector in the shock normal direction. It follows that

$$\tilde{u}_1 = \frac{1}{m} [u_1 \zeta_x \hat{i} + v_1 \zeta_y \hat{j} + w_1 \zeta_z \hat{k}] \quad (43)$$

where

$$m = (\zeta_x^2 + \zeta_y^2 + \zeta_z^2)^{1/2} \quad (44)$$

and u_1, v_1, w_1 are the components of \overline{q}_1 and $\zeta_x, \zeta_y, \zeta_z$ are the coordinate metrics. The variable \overline{u}_{ss_1} can be obtained directly for a perfect gas from the relation

$$|u_{ss_1}| = \sqrt{\frac{p_1}{2\rho_1} \left[(\gamma + 1) \frac{p_2}{p_1} + (\gamma - 1) \right]} \quad (45)$$

and its known direction. The replacement formulation including real gas effects requires two steps. First, the density behind the shock is obtained from the relation

$$\rho_2 = \rho_1 \left[\frac{p_1 + (1 + 2\phi_2) p_2}{p_2 + (1 + 2\phi_1) p_1} \right] \quad (46)$$

which is the real gas analog of the perfect gas relation

$$\rho_2 = \rho_1 \left[\frac{(\gamma + 1)p_2 + (\gamma - 1)p_1}{(\gamma + 1)p_1 + (\gamma - 1)p_2} \right] \quad (47)$$

which also appears in the perfect gas formulation. Having obtained both the pressure and density behind the shock, $|u_{ss1}|$ is readily obtained from the Rankine-Hugoniot relation

$$|u_{ss1}| = \sqrt{\left(\frac{\rho_2}{\rho_1}\right) \left(\frac{p_2 - p_1}{\rho_2 - \rho_1}\right)} \quad (48)$$

or in final form

$$\vec{u}_{ss1} = -|u_{ss1}| [\zeta_x \hat{i} + \zeta_y \hat{j} + \zeta_z \hat{k}] / m \quad (49)$$

The velocity component \vec{u}_{ss} can also be evaluated behind the shock (i.e., \vec{u}_{ss2}). This variable is interpreted as the shock normal component of velocity required to maintain a steady-state shock of pressure ratio p_2/p_1 . It is evaluated from the relation

$$\vec{u}_{ss2} = -\frac{\rho_1}{\rho_2} \vec{u}_{ss1} \quad (50)$$

or

$$\vec{u}_{ss_2} = \frac{\rho_1 |u_{ss_1}|}{\rho_2 m} [\zeta_x \hat{i} + \zeta_y \hat{j} + \zeta_z \hat{k}] \quad (51)$$

The components of velocity tangent to the shock wave (\vec{v}_1, \vec{v}_2) are given by

$$\vec{v}_1 = \vec{v}_2 = \vec{q}_1 - \vec{u}_1 \quad (52)$$

or

$$\vec{v}_2 = u_1 \left(1 - \frac{\zeta_x}{m}\right) \hat{i} + v_1 \left(1 - \frac{\zeta_y}{m}\right) \hat{j} + w_1 \left(1 - \frac{\zeta_z}{m}\right) \hat{k} \quad (53)$$

which completes the evaluation of the components needed to evaluate \vec{q}_2 .

The velocity components are added in the manner illustrated in Fig. 1 to yield

$$\vec{q}_2 = \vec{u}_{ss_2} + \vec{v}_2 + \vec{q}_s \quad (54)$$

which becomes

$$\vec{q}_2 = -\frac{\rho_1}{\rho_2} \vec{u}_{ss_1} + \vec{q}_1 - \vec{u}_1 + \vec{u}_{ss_1} + \vec{u}_1 = \vec{q}_1 + \vec{u}_{ss_1} \left(1 - \frac{\rho_1}{\rho_2}\right) \quad (55)$$

after substituting in Eqs. (41), (49), and (51). The components of \vec{q}_2 are readily evaluated from Eqs. (48) and (54) as

$$\left. \begin{aligned} u_2 &= u_1 + B \zeta_x / m \\ v_2 &= v_1 + B \zeta_y / m \\ w_2 &= w_1 + B \zeta_z / m \end{aligned} \right\} \quad (56)$$

where

$$B = - \sqrt{\left(\frac{\rho_2}{\rho_1}\right) \left(\frac{p_2 - p_1}{\rho_2 - \rho_1}\right) \left(1 - \frac{\rho_1}{\rho_2}\right)} \quad (57)$$

Eq. (56) is identical to the analogous relation in the perfect gas formulation. Equation (57) is significantly different in that B is related to perfect gas variables as

$$B = 2 \sqrt{\gamma \frac{p_1}{\rho_1}} \frac{\left\{ \frac{1}{2\gamma} \left[(\gamma + 1) \frac{p_2}{p_1} + (\gamma - 1) \right] - 1 \right\}}{(\gamma + 1) \sqrt{\frac{1}{2\gamma} \left[(\gamma + 1) \frac{p_2}{p_1} + (\gamma - 1) \right]}} \quad (58)$$

Equations (47), (56), and (57) represent the changes to the unsteady flow shock fitting procedure associated with real gas effects. The remaining formulation is unchanged from the perfect gas formulation as described by Kutler and Pedelty.³

For the PNS application, the velocity component normal to the shock is obtained from a real gas version of the Rankine-Hugoniot relation

$$|\tilde{u}_1| = \sqrt{\frac{(p_1 - p_2) [p_1 + (1 + 2\phi_2) p_2]}{2\rho_1 (\phi_1 p_1 - \phi_2 p_2)}} \quad (59)$$

which is used in place of the equivalent perfect gas relation

$$|\tilde{u}_1| = \sqrt{\frac{(\gamma + 1) p_2 + (\gamma - 1) p_1}{2\rho_1}} \quad (60)$$

The metrics at the shock are obtained either from coordinate transformation relations (ζ_x , η_x , ξ_x) or from numerical

differentiation (for $\zeta_y, \zeta_z, \eta_y, \eta_z, \xi_y, \xi_z$) in the crossflow plane. The formulation for these relations is unchanged by the introduction of real gas effects, e.g.

$$\zeta_x = \frac{u_1(w_1\zeta_z + v_1\zeta_y) + \sqrt{\tilde{u}_1^2[(w_1\zeta_z + v_1\zeta_y)^2 - (\tilde{u}_1^2 - u_1^2)(\zeta_z^2 + \zeta_y^2)]}}{(\tilde{u}_1^2 - u_1^2)} \quad (61)$$

and

$$\eta_x = \zeta_x \left(\frac{\zeta_y \eta_y + \zeta_z \eta_z}{\zeta_y^2 + \zeta_z^2} \right) \quad (62)$$

A typical point on the shock is propagated using the following equations:

$$\left. \begin{aligned} z^{j+1} &= z^j + z_\xi^j \Delta\xi \\ y^{j+1} &= y^j + y_\xi^j \Delta\xi \end{aligned} \right\} \quad (63)$$

where

$$\left. \begin{aligned} z_\xi &= (\eta_y \zeta_x - \eta_x \zeta_y) / J \\ y_\xi &= (\eta_x \zeta_z - \eta_z \zeta_x) / J \end{aligned} \right\} \quad (64)$$

The density component behind the shock wave is calculated from the real gas relation

$$\rho_2 = \rho_1 \left[\frac{p_1 + (1 + 2\phi_2)p_2}{p_2 + (1 + 2\phi_1)p_1} \right] \quad (65)$$

which is used in place of the perfect gas relation

$$\rho_2 = \rho_1 \left[\frac{(\gamma + 1)p_2 + (\gamma - 1)p_1}{(\gamma + 1)p_1 + (\gamma - 1)p_2} \right] \quad (66)$$

and, finally, the velocity components behind the shock are found from

$$\begin{aligned}u_2 &= u_1 + B_{ss} \zeta_x/m \\v_2 &= v_1 + B_{ss} \zeta_y/m \\w_2 &= w_1 + B_{ss} \zeta_z/m\end{aligned}\tag{67}$$

where

$$B_{ss} = |\tilde{u}_1|(1 - \rho_1/\rho_2)\tag{68}$$

which completes the formulation.

5. Implementation in PNS Code

The flowfield procedures obtain real gas properties from tabulations stored in memory. The data in the tables is generated prior to and separate from the flowfield calculation. Tabular data for air was obtained from well established compilations^{4,5} and is presently included in the code.* Data for environments other than air can be generated using a procedure discussed elsewhere⁶. The material presented herein discusses the data requirements, the format of the tables, the searching procedures employed, and the interpolation relations used to obtain data between table entries.

The independent variables employed are $\log_{10} p$ and $\log_{10} \rho/\rho_0$, where ρ_0 is the density of air at standard conditions ($\rho_0 = 1.225 \times 10^{-3} \text{ gm/cm}^3$). The dependent variables include four thermodynamic variables, three transport properties, and two partial derivatives of transport properties. The thermodynamic properties appear in the format ϕ , $\frac{\rho RT}{p}$, $\frac{\rho a^2}{p}$, C_{p_f}/C_p . The transport properties appear in the format μ , Pr , and Sc . In addition,

* The real gas viscosity data never reduces to the Sutherland formula exactly, so small differences will always exist between real gas and perfect gas predictions.

entropy is related to pressure and density via the relation

$$\left[\frac{p}{\rho_0} \right]^{\gamma_s} = \frac{p}{\rho} \exp \left\{ (\gamma_s - 1) \frac{(S_0 - S)}{R} \right\} \quad (69)$$

where the effective specific heat ratio γ_s is also tabulated as a function of $\log_{10} \frac{p}{p_0}$ and $\log_{10} \frac{\rho}{\rho_0}$. For air the reference condition $\frac{S_0}{R}$ was set to 23.5372.

Each of the tabulated properties is evaluated at the last marching step as known functions of pressure and density, then frozen and treated as being independent of x (or ξ) in the evaluation of the equations at the current marching step. The approach is successful because each of the tabulated properties is a slowly varying function of axial distance.

SECTION III

CALCULATIONS

Calculations have been carried out for a single model geometry flying at three interesting flight conditions. The results obtained allow an assessment to be made of the effects of the real gas equation of state and transport properties on the prediction of the aerodynamic and aerothermodynamic environments.

1. Model Geometry

The model consists of a cone-cylinder with an 8 degree half angle conical tip, 0.075-inch radius spherical nose bluntness, 1.4 inch diameter body and an overall length of 11.20 inches (eight caliber).

2. Flight Conditions

The flight conditions for each of the three cases considered are given in Table 1.

Table 1
Flight Conditions

	Case Number		
	1	2	3
Mach Number	6	8	10
Angle of Attack (deg.)	2	2	2
Free Stream			
Static Temp. ($^{\circ}\text{R}$)	530	530	530
Static Pressure (atm)	1	1	1
Wall Temperature ($^{\circ}\text{R}$)	530	530	530
Reynolds No. ($\text{in}^{-1} \times 10^{-6}$)	3.615	4.82	6.025

3. Surface Grid

The surface geometry was generated using the FLAG=2 option (see Ref. 2), plus a surface geometry file having 45 points in the circumferential half-plane and, finally, used in conjunction with a virtual origin situated .45865 inch upstream of the nose (used to generate the spherical cap and the conical surface). All output from the computer is referenced to the virtual origin, not the nose of the model.

4. Starting Conditions

The blunt body code of Kutler et al³ was used to generate a flowfield solution over the spherical cap of the model for each case considered. The output from each solution consists of two planes of data to be used to start PNS code calculations. For each of the cases considered, the downstream data plane was situated at a distance $x = .0587$ inch from the nose which is just upstream of the tangency point at $x = .06456$ inch from the nose. At the starting plane, the surface slope is at an angle of 12.55° to the axis, so that most of the very rapid expansion associated with the nose cap is over.

The Kutler et al³ blunt body code is a perfect gas code which was used only because no alternative real gas code of this type was available. Consequently, the starting solutions were always somewhat inconsistent with the real gas PNS solutions. The sensitivity of the Case 3 solution to this inconsistency was assessed as part of the calculation matrix.

5. Downstream Solutions

An initial set of solutions was calculated to establish the validity of the prediction procedure. Our objective was to assess the sensitivity

of the solutions to the arbitrary inputs which must be adopted in making calculations. The following issues are of particular concern and were addressed:

- (1) Does either the position of the starting plane of data and/or the interpolations needed to start the calculations have any lasting effect on the nature of the downstream solution?
- (2) It is necessary to introduce arbitrary transition regions to gradually change the flowfield from perfect gas to real gas and/or from laminar to turbulent flow. Do the features of the transition region selected have any lasting effect on the nature of the downstream solution? The transition region was never allowed to extend beyond .1787 inch downstream from the nose.
- (3) Damping and/or smoothing parameters must be selected and employed to stabilize calculations. Do they have any lasting effect on the nature of the downstream solutions?
- (4) The distance from the wall to the first grid point off the wall (DS) must be selected arbitrarily and must be small enough to maintain accuracy but large enough to maintain stability. Can suitable values be found? An initial DS of .0006 inch was selected for laminar flows while .0004 inch was selected for turbulent flows.

It was found that the selection of the damping and smoothing parameters have, by far, the most important effect on the nature of the downstream solution. Indeed, the selection of excessive damping parameters (particularly ϵ_A and ϵ_B , Ref 2) were found to change the qualitative features of

solutions. Values of $\epsilon_A = .05$ and $\epsilon_B = .10$ yielded acceptable solutions, both in terms of accuracy and stability, and were selected for the final calculations. Changing the other arbitrary inputs tended to move the solutions around a little. Fortunately, such changes tended to have the same kinds of effects on both the perfect gas and the real gas solutions and, consequently, were not of much concern for the purposes of the present study.

Flowfields over slender, spherically capped cones have been studied by a number of investigators. The results of Harris⁷ are presented in Figure 2 as an example where $\alpha = 0$, $R_N = .5$ inch, $M_\infty = 8$ and the conical half angle is 7 degrees. As shown, the pressure drops rapidly around the nose cap, overexpands, then recovers slowly to the conical pressure. The recovery to the conical pressure can be measured in tens of nose diameters, an effect associated with the strong entropy layer in the shock layer. Increasing (or decreasing) either the angle of attack or the conical half angle decreases (or increases) the distance required to recover the conical pressure.

Axial pressure distributions obtained in the present study are presented in Figures 3, 4 and 8. They all display the expected qualitative features. Moreover, the $M_\infty = 8$ pressure distributions given in Figure 8 are in acceptable agreement with the Figure 2 results considering the differences in Reynold's Number, angle of attack and cone half angle.

The $M_\infty = 10$ solutions are presented in Figures 3 to 6 in the forebody region. It was felt that real gas effects would be present here if they are going to be present anywhere. An examination of the starting plane of data showed that real gas effects were clearly important there. Real gas pressures differed by as much as 25% from their perfect gas counterparts.

However, by the time the flow is allowed to expand and cool through the transition region and progress downstream far enough to establish a valid PNS solution, the effect is never more than a few percent. Pressure distributions for the two pitch planes are given for laminar flow in Figure 3. Pressure distributions for the two pitch planes are given for turbulent flow in Figure 4. Similar effects are shown for heat transfer in Figures 5 and 6.

The fact that the heat transfer rates and pressure distributions are changed very little does not imply that the structure of the shock layer is virtually unchanged, however. To illustrate the point, the temperature distribution across the shock layer for $x = 2.053$ inches at the windward pitch plane is shown in Figure 7. As shown, the perfect gas temperatures are about 450°R higher than the real gas temperatures at the maximum temperature of the entropy layer. However, both perfect gas and real gas distributions become nearly identical at both shock front and wall boundaries.

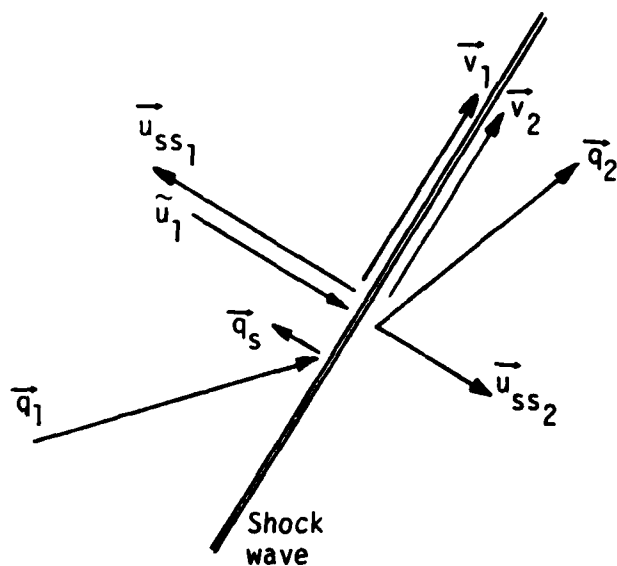
To complete the calculation matrix, the $M_{\infty} = 6$ and $M_{\infty} = 8$ cases were run and are presented in Figures 8 and 9 along with the entire $M_{\infty} = 10$ results. The real gas effects on the $M_{\infty} = 10$ is small, while the effects of real gas on the other two solutions cannot be separated from uncertainties in the solution procedure and can be viewed as negligible.

SECTION IV

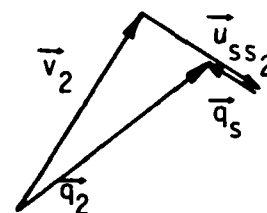
CONCLUDING REMARKS

On the basis of the present study, the following conclusions have been reached regarding the real gas effects on the prediction of flow-fields about Army projectiles:

- o There appears to be a moderately significant effect on the nose of the vehicle where temperatures and pressures are high and molecular dissociation is enhanced. However, this conclusion is tentative since the PNS code used in the present study is not applicable to the nose cap region of the flow.
- o Real gas effects change the heating rates and pressure distributions by a few percent. Even this small effect disappears after 1 or 2 inches of axial length.
- o Real gas effects are important in determining the interior structure of the shock layer where the temperatures can be changed significantly.



(a) Sign Convention for Velocity Vectors



(b) Components of Particle Velocity, \vec{q}_2

Figure 1. Shock Wave Notation

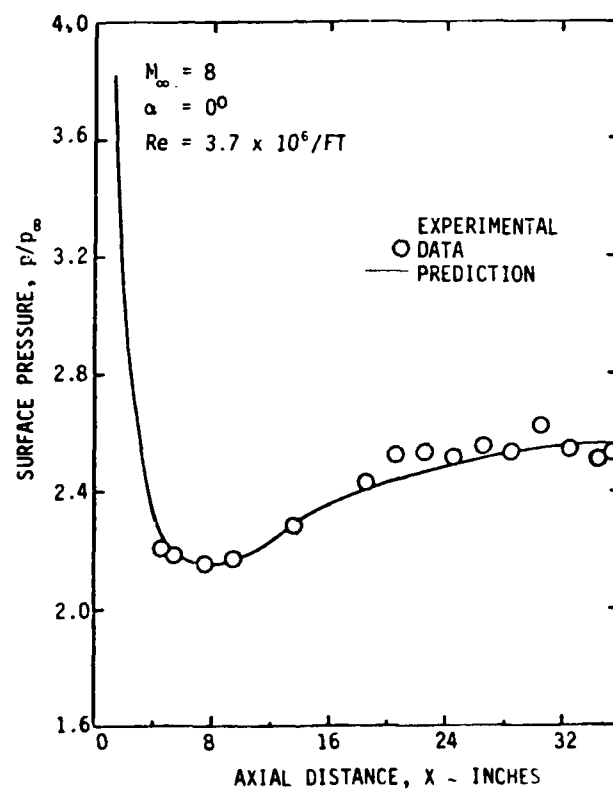


Figure 2. Pressure Distribution on 7° Sphere Cone at $\alpha = 0^\circ$ from Harris⁷

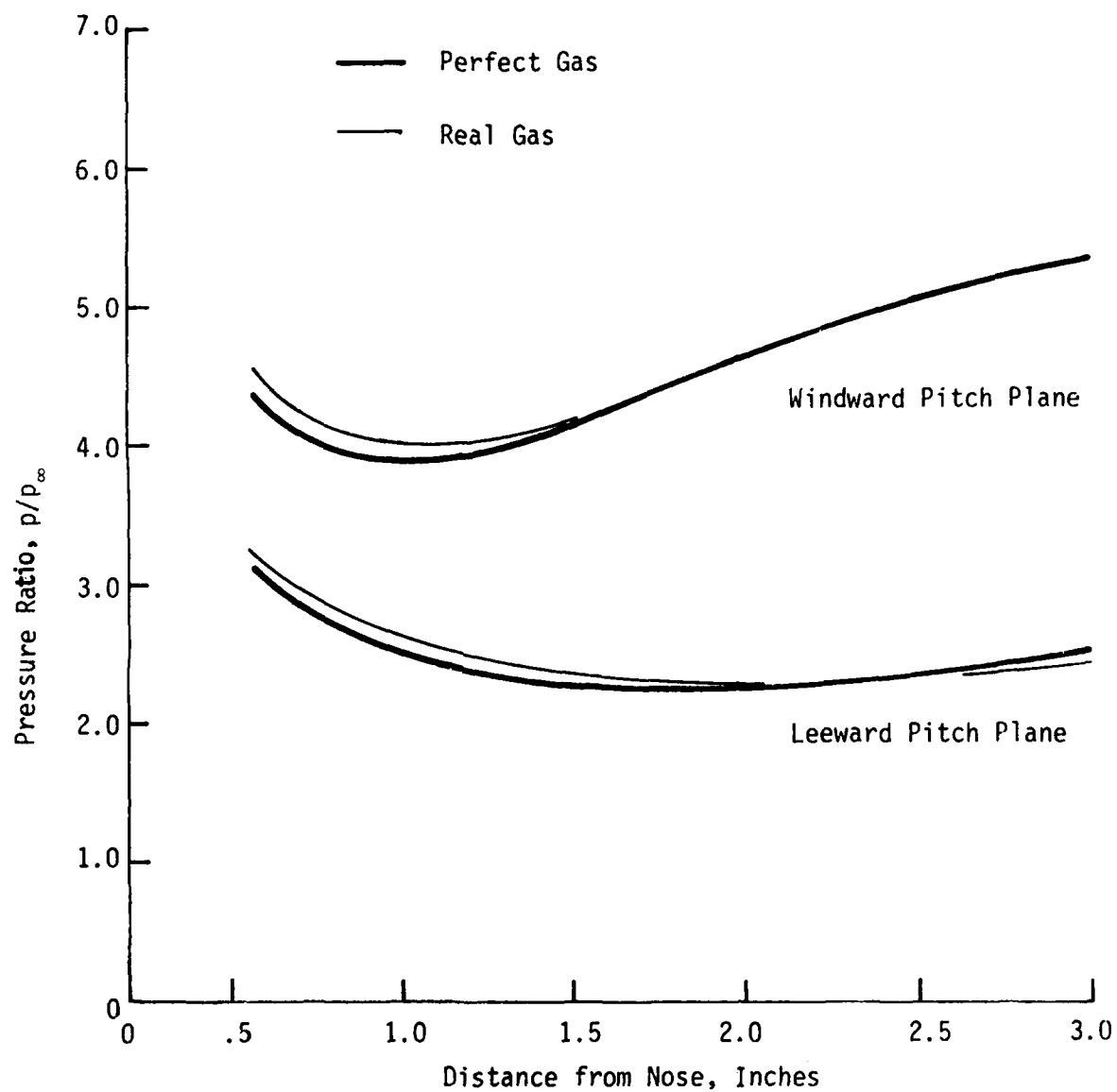


Figure 3. Pressure Distribution for Case 3 ($M = 10$) Showing Real Gas Effects for Laminar Flow.

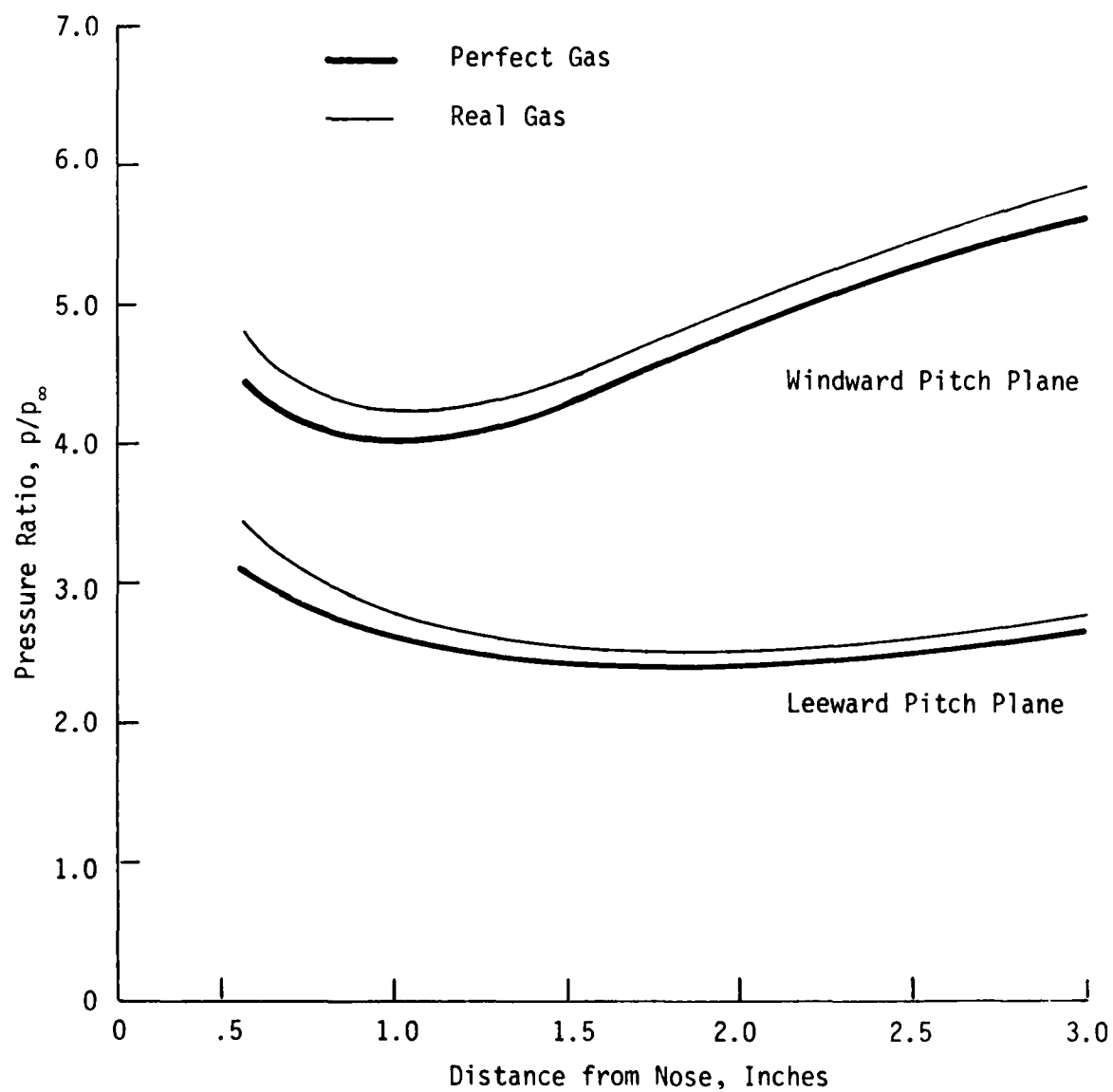


Figure 4. Pressure Distribution for Case 3 ($M = 10$) Showing Real Gas Effects for Turbulent Flow.

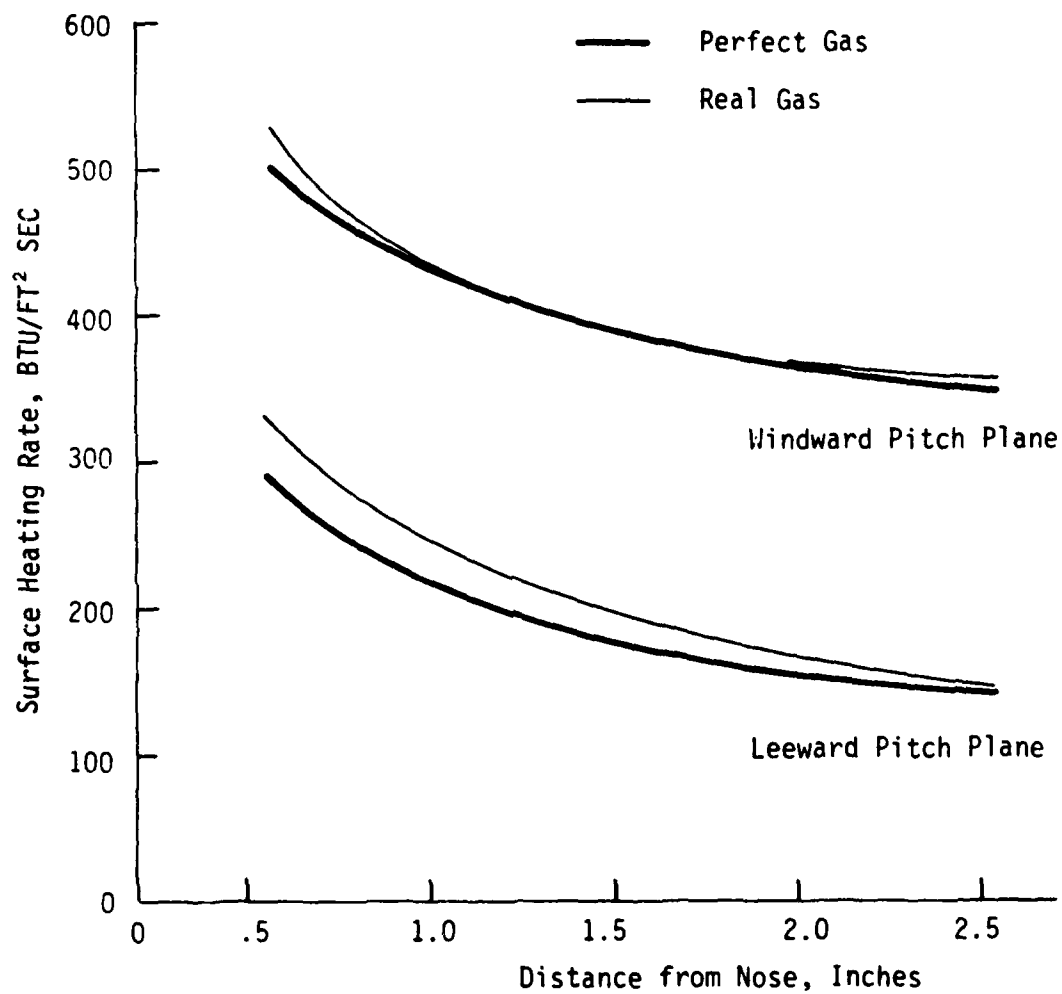


Figure 5. Heat Transfer for Case 3 ($M = 10$) Showing Real Gas Effects for Laminar Flow.

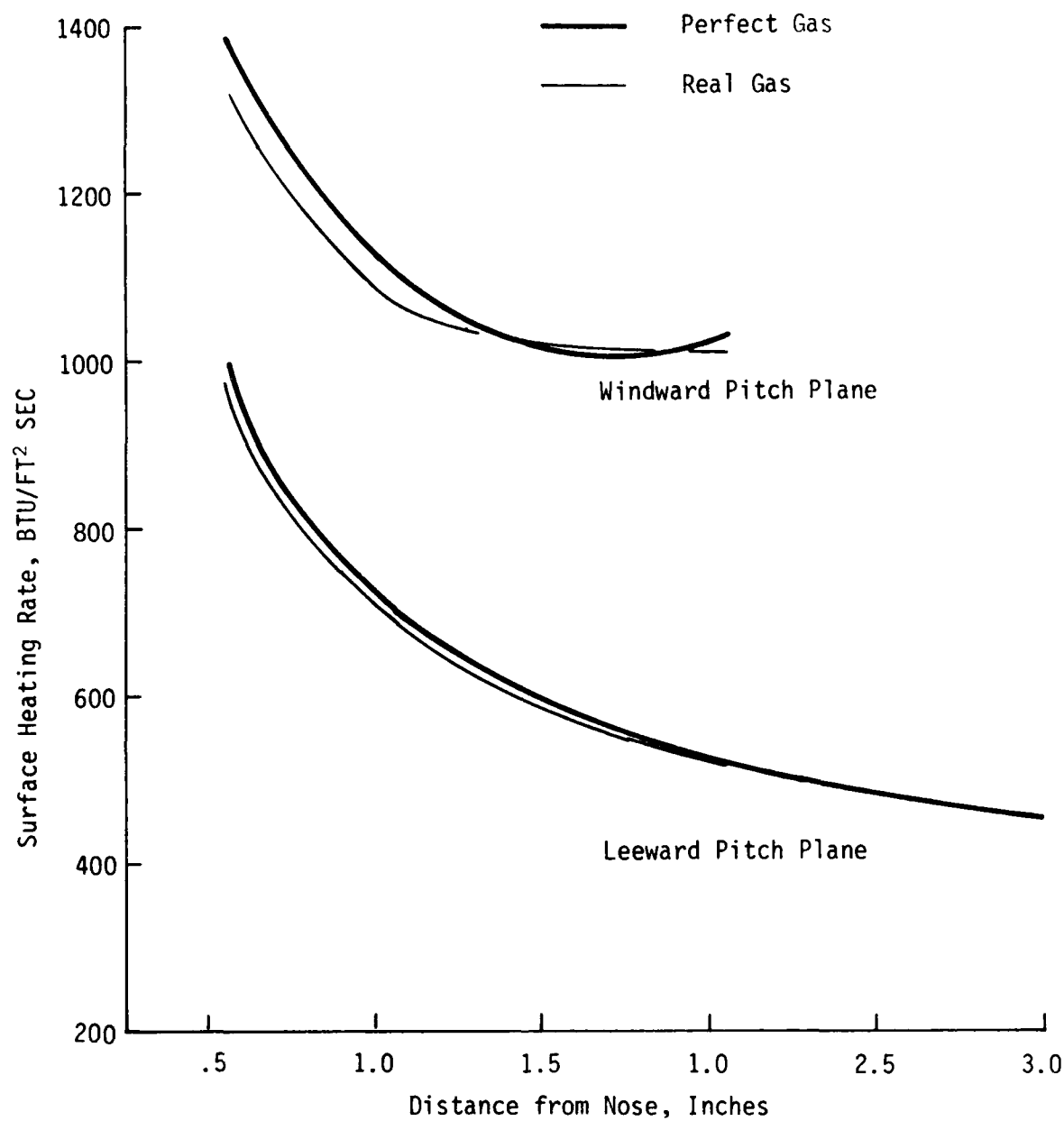


Figure 6. Heat Transfer for Case 3 ($M = 10$) Showing Real Gas Effects for Turbulent Flow.

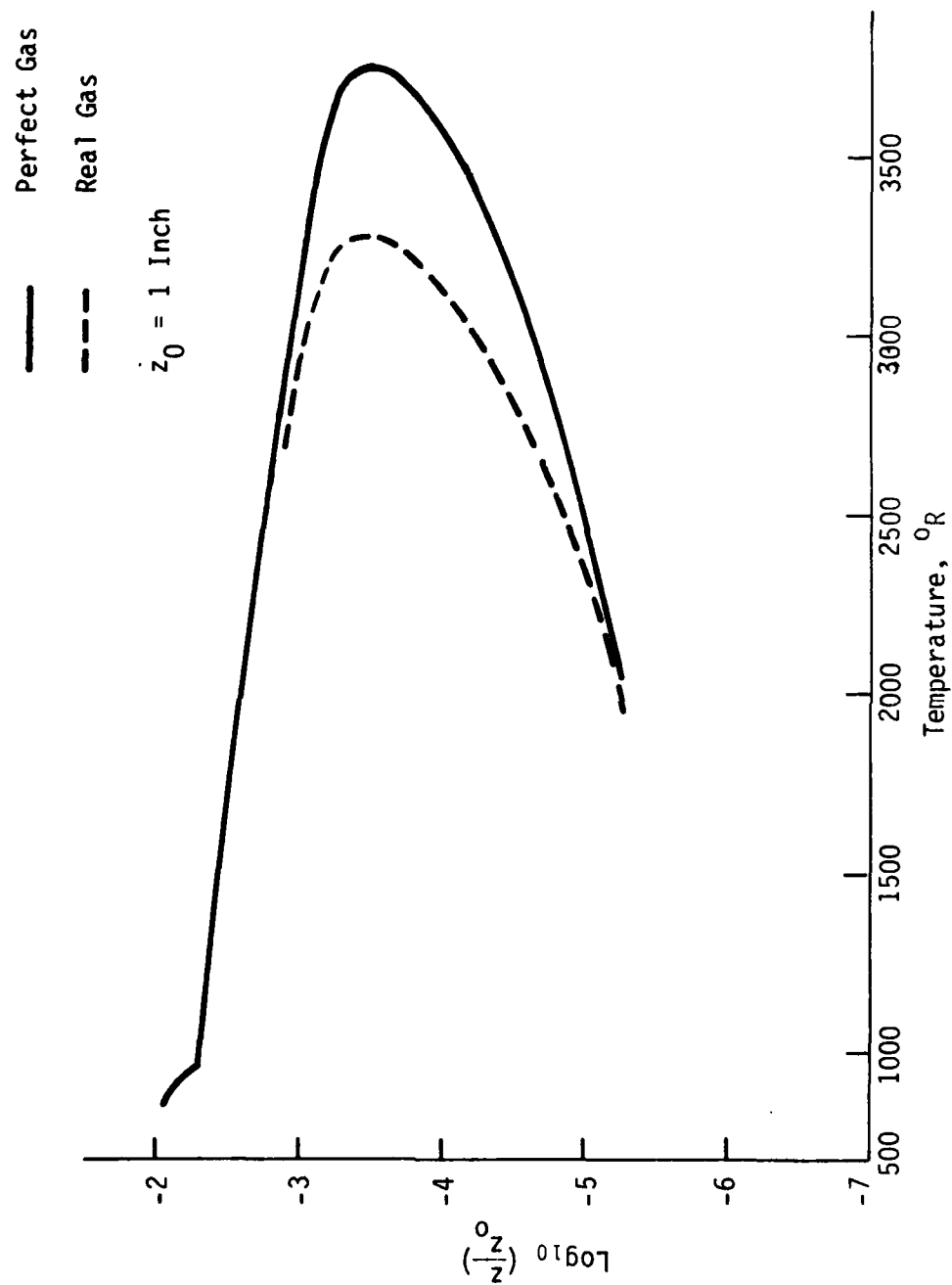


Figure 7. Temperature Distribution Across Shock Layer for $x = 2.053$ Inches at Windward Pitch Plane (Case 3).

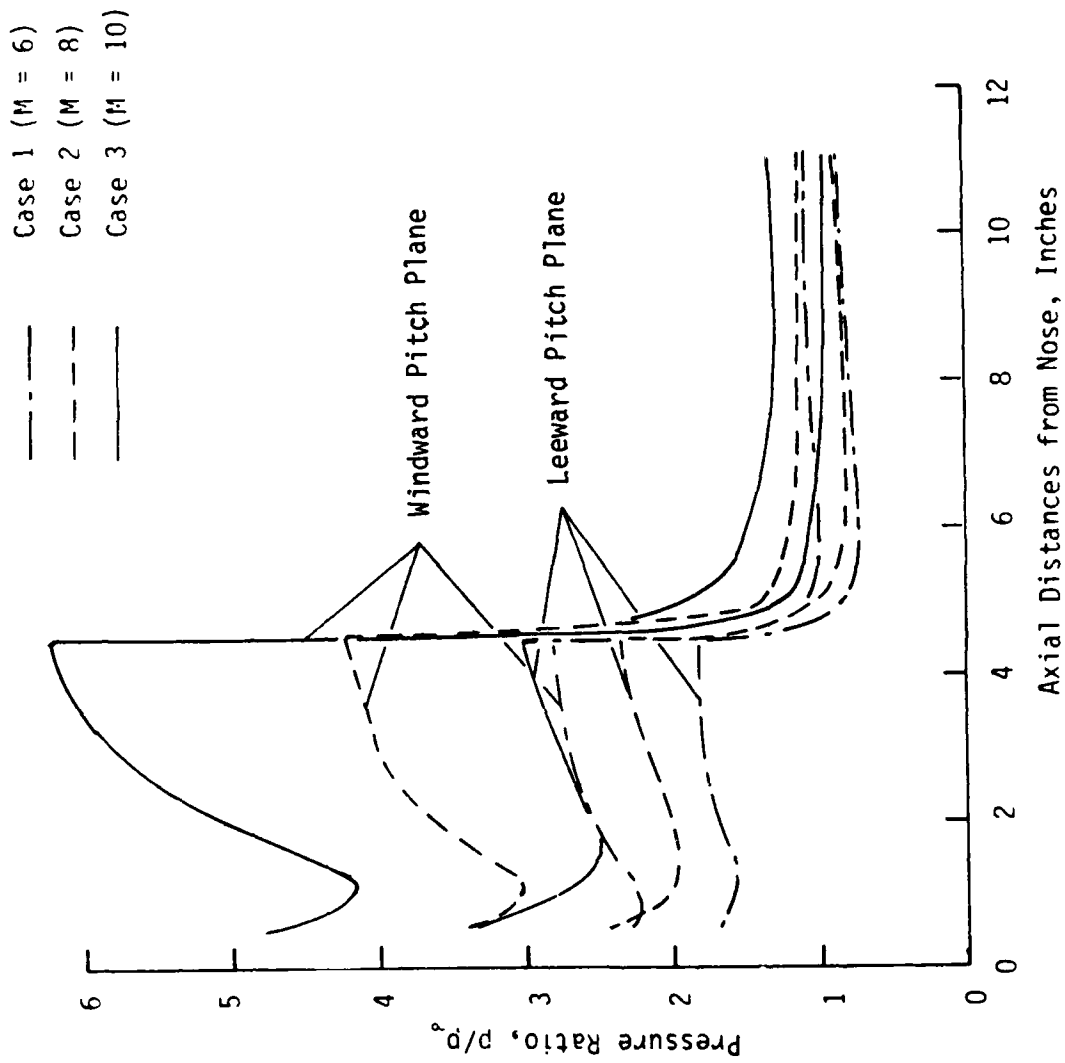


Figure 8. Real Gas Axial Pressure Distribution for Cases 1, 2 and 3.

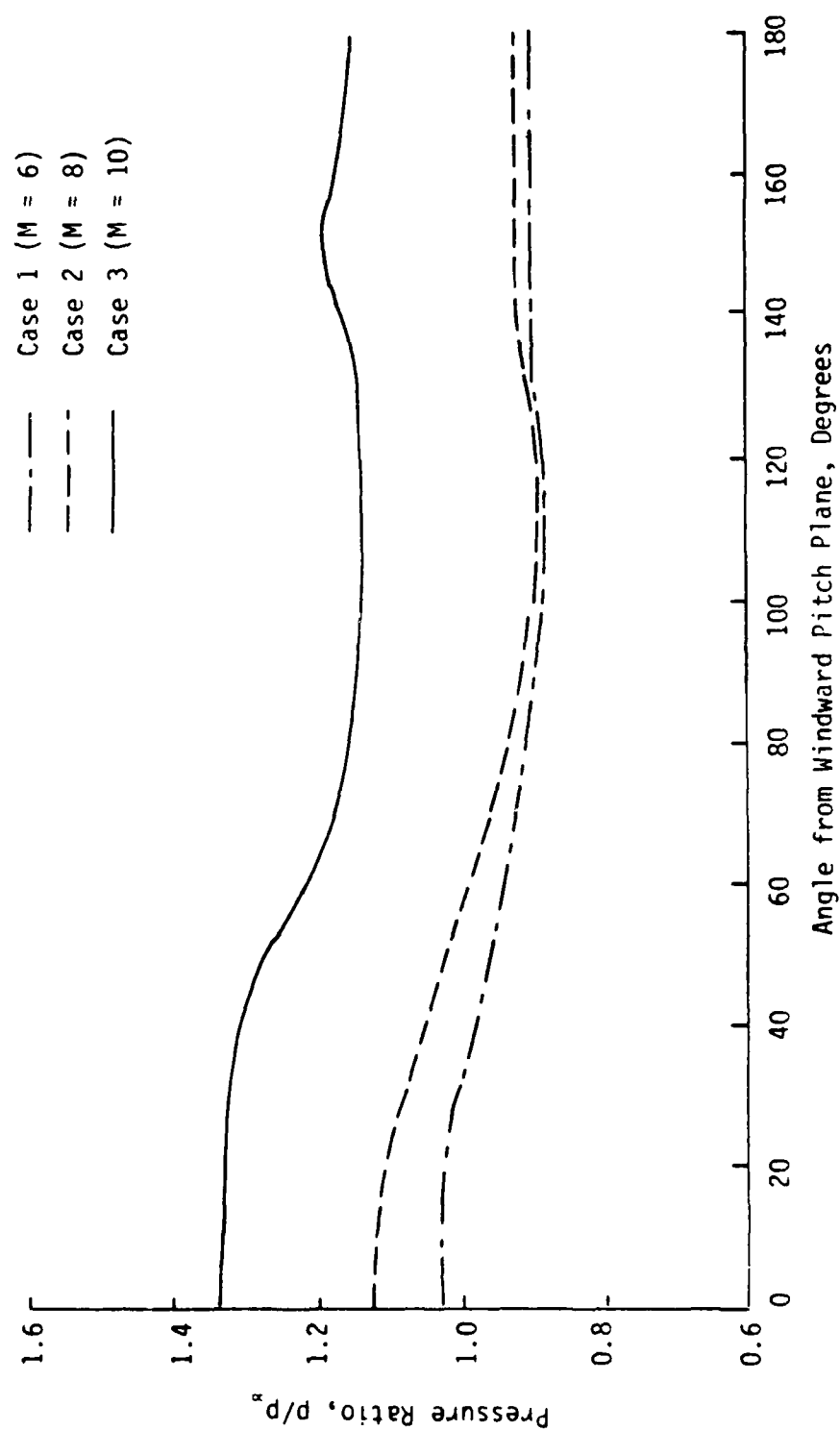


Figure 9. Real Gas Circumferential Pressure Distribution at $\gamma = 11.2$ Inches for Cases 1, 2 and 3.

REFERENCES

1. Nicolet, W.E., Srinivasan, G. R., and Shanks, S.P., "AFWAL PNS Code: Flowfield Calculations at Ground Test Conditions and Reformulation for Flight Applications," Report 82-01, Thermal Sciences, Inc., Sunnyvale, California, December 1982.
2. Shanks, S.P., Srinivasan, G.R., and Nicolet, W.E., "AFWAL Parabolized Navier-Stokes Code: Formulation and User's Manual," AFWAL-TR-82-3034, Flow Simulations, Sunnyvale, California, June 1982.
3. Kutler, P., Pedelty, J.A., and Pulliam T.H., "Supersonic Flow Over Three-Dimensional Ablated Nosed Tips Using an Unsteady Implicit Numerical Procedure," AIAA Paper 80-0063, January 1980.
4. Peng, T.C., and Pendrogh, A.L., "An Improved Calculation of Gas Properties at High Temperatures: Air," Paper No. 1995-61, Fourth Biennial Gas Dynamics Symposium, American Rocket Society, Northwestern University, Evanston, Illinois, August 23-25, 1961. Also, Document No. DZ-11722, Category Code No. 81205, Boeing Airplane Company, Seattle, Washington, February 1962.
5. Hilsenrath, J., and Klein, M., "Tables of Thermodynamic Properties of Air in Chemical Equilibrium Including Second Virial Corrections from 1,500 °K to 15,000 °K," Report No. AEDC-TR-65-58, Arnold Engineering Development Center, Tennessee, March 1965.
6. Powars, C.A., and Kendall, R.M., "User's Manual - Aerotherm Chemical Equilibrium (ACE) Computer Program," Report (without a number), Acurex Corporation, Mountain View, California, May 1969.
7. Harris, T.B., "An Efficient Method for Supersonic Viscous Flowfield Calculations," Paper AIAA-83-0222 presented at 21st Aerospace Sciences Meeting, Reno, Nevada, January 1983.

DISTRIBUTION LIST

<u>No. of Copies</u>	<u>Organization</u>	<u>No. of Copies</u>	<u>Organization</u>
12	Administrator Defense Technical Info Center ATTN: DTIC-DDA Cameron Station Alexandria, VA 22314	1	Director US Army Air Mobility Research and Development Laboratory Ames Research Center Moffett Field, CA 94035
1	Commander US Army Materiel Development and Readiness Command ATTN: DRCDMD-ST 5001 Eisenhower Avenue Alexandria, VA 22333	1	Commander US Army Communications Rsch and Development Command ATTN: DRSEL-ATDD Fort Monmouth, NJ 07703
9	Commander US Army Armament Research and Development Command ATTN: DRSMC-TDC DRSMC-TSS DRSMC-LCA-F Mr. D. Mertz Mr. E. Falkowski Mr. A. Loeb Mr. R. Klien Mr. S. Kahn Mr. H. Hudgins Dover, NJ 07801	1	Commander US Army Electronics Research and Development Command Technical Support Activity ATTN: DELSD-L Fort Monmouth, NJ 07703
1	Commander US Army Armament Materiel Readiness Command ATTN: DRSAR-LEP-L Rock Island, IL 61299	2	Commander US Army Missile Command ATTN: DRSMI-R DRSMI-RDK Mr. R. Deep Redstone Arsenal, AL 35898
1	Director US Army Armament Research and Development Command Benet Weapons Laboratory ATTN: DRDAR-LCB-TL Watervliet, NY 12189	1	Commander US Army Missile Command ATTN: DRSMI-YDL Redstone Arsenal, AL 35898
1	Commander US Army Aviation Research and Development Command ATTN: DRDAV-E 4300 Goodfellow Blvd. St. Louis, MO 63120	1	Commander US Army Tank Automotive Command ATTN: DRSTA-TSL Warren, MI 48090
		1	Director US Army TRADOC Systems Analysis Activity ATTN: ATAA-SL, Tech Lib White Sands Missile Range NM 88002

DISTRIBUTION LIST

<u>No. of Copies</u>	<u>Organization</u>	<u>No. of Copies</u>	<u>Organization</u>
1	Commander US Army Research Office P. O. Box 12211 Research Triangle Park NC 27709	2	Commandant US Army Infantry School ATTN: ATSH-CD-CSO-OR Fort Benning, GA 31905
1	Commander US Naval Air Systems Command ATTN: AIR-604 Washington, D. C. 20360	1	ACUREX Corporation/Aerotherm ATTN: Dr. M. J. Abbett 485 Clyde Avenue Mountain View CA 94042
2	Commander David W. Taylor Naval Ship Research and Development Center ATTN: Dr. S. de los Santos Mr. Stanley Gottlieb Bethesda, Maryland 20084	1	AVCO Systems Division Dr. W. Reinecke 201 Lowell Street Wilmington, MA 01887
4	Commander US Naval Surface Weapons Center ATTN: Dr. T. Clare, Code DK20 Mr. P. Daniels Mr. D. A. Jones, III Mr. L. Mason Dahlgren, VA 22448	1	Nielsen Engineering & Research, Inc. ATTN: Dr. S. Stahara 510 Clyde Avenue Mountain View, CA 94043
4	Commander US Naval Surface Weapons Center ATTN: Code 312 Dr. W. Yanta Code R44 Dr. C. Hsieh Dr. T. Zien Mr. U. Jettmar Silver Spring, MD 20910	2	Thermal Sciences, Inc. 292 Gibraltar Dr., Suite A-4 Sunnyvale, CA 94086
1	Commander US Naval Weapons Center ATTN: Code 3431, Tech Lib China Lake, CA 93555	2	Sandia Laboratories ATTN: Technical Staff, Dr. W. L. Oberkampf Aeroballistics Division 5631, H. R. Vaughn Albuquerque, NM 87115
1	AFWL/SUL Kirtland AFB, NM 87117	1	Bendix Guided Systems Division ATTN: MS 2/17A, S. Wasserman Teterboro, NJ 07608
		1	Massachusetts Institute of Technology ATTN: Tech Library 77 Massachusetts Avenue Cambridge, MA 02139
		1	University of Delaware Mechanical and Aerospace Engineering Department ATTN: Dr. J. E. Danberg Newark, DE 19711

Aberdeen Proving Ground

Dir, USAMSAA

ATTN: DRXSY-D
DRXSY-MP, H. Cohen

Cdr, USATECOM

ATTN: DRSTE-TO-F

Dir, USACSL, Bldg. E3516, EA

ATTN: DRDAR-CLB-PA
DRDAR-CLN
DRDAR-CLJ-L

USER EVALUATION OF REPORT

Please take a few minutes to answer the questions below; tear out this sheet, fold as indicated, staple or tape closed, and place in the mail. Your comments will provide us with information for improving future reports.

1. BRL Report Number _____

2. Does this report satisfy a need? (Comment on purpose, related project, or other area of interest for which report will be used.)

3. How, specifically, is the report being used? (Information source, design data or procedure, management procedure, source of ideas, etc.) _____

4. Has the information in this report led to any quantitative savings as far as man-hours/contract dollars saved, operating costs avoided, efficiencies achieved, etc.? If so, please elaborate.

5. General Comments (Indicate what you think should be changed to make this report and future reports of this type more responsive to your needs, more usable, improve readability, etc.) _____

6. If you would like to be contacted by the personnel who prepared this report to raise specific questions or discuss the topic, please fill in the following information.

Name: _____

Telephone Number: _____

Organization Address: _____

----- FOLD HERE -----

Director
US Army Ballistic Research Laboratory
ATTN: DRDAR-BLA-S
Aberdeen Proving Ground, MD 21005

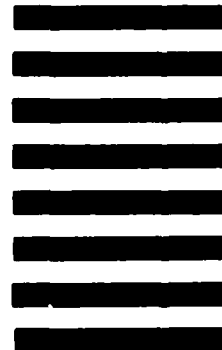


NO POSTAGE
NECESSARY
IF MAILED
IN THE
UNITED STATES

OFFICIAL BUSINESS
PENALTY FOR PRIVATE USE, \$300

BUSINESS REPLY MAIL
FIRST CLASS PERMIT NO 12062 WASHINGTON, DC
POSTAGE WILL BE PAID BY DEPARTMENT OF THE ARMY

Director
US Army Ballistic Research Laboratory
ATTN: DRDAR-BLA-S
Aberdeen Proving Ground, MD 21005



----- FOLD HERE -----

END

FILMED

12-83

DTIC